INFRARED SIGNATURES OF BONDED INTERFACES FOR THE REPAIR OF PRIMARY STRUCTURES IN COMPOSITE MATERIALS

M. Barus[1,2], F. Collombet[1], H. Welemane[2],
L. Crouzeix[1], A. Cantarel[3], Y. Grunevald[4], V. Nassiet[2], M.L. Pastor[3]

[1]Université de Toulouse, UT3, IUT-ICA, 3 rue Caroline Aigle, 31400 Toulouse CEDEX 04, France

[2]Université de Toulouse, INP, ENIT-LGP, 47 Av.Azereix, BP 1629, 65016 Tarbes Cedex, France

[3]Université de Toulouse, UT3, IUT-ICA, 1 rue Lautréamont, BP 1624, 65016 Tarbes Cedex, France

[4]Composites Expertise & Solutions (CES), 4 rue Georges Vallerey, 31320 Castanet Tolosan France

Keywords: Composite repair, Infrared thermography, Bonding certification

ABSTRACT

This paper deals with the use of infrared thermography for the reliability evaluation of bonded repaired composite structures. To address such issue, the present work intends to characterize a heat flow load by inverse identification. In this way, a specific experimental bench is developed to carry out thermal tests under controlled conditions. Moreover, the FEMU technique is adopted to identify the heat flow amplitude by means of correlation between experimental and numerical surface temperature fields. Such procedure is used on metallics coupons to identify the heat flow and is validated on carbon fiber laminates with different lay up.

1 Introduction

Since the design of planes built with very large and non-dismantle composite parts (body or wing of A350 Airbus for example [1]), the repair of primary structures by bonded composite patches becomes more and more important. Effectively, this technical solution provides an uniform diffusion of stresses into the adhesive joint. Yet, despite many studies [2, 3, 4], this type of repair still remains uncertified because of several difficulties. First no methodology allows to evaluate its reliability level. Especially, the adhesive strength between the primary structure and the composite patch needs to be effective in order to ensure the involvement of the repaired part as a structural reinforcement [5]. Then this technology suffers from a lack of background regarding the ageing and behaviour in fatigue.

Existing studies on bonded structures deal essentially with thickness [6], stiffness [7] and delamination checking [8], as well as the determination of the optimal overlap length [9]. They are mainly performed on coupons and, especially, on the slice of specimens that show all parts of the problem. However, repair is a closed assembly in an industrial context and in this case, measurements on the slice are impossible. So, the ambition of the following study is to characterize the repair quality of primary structures by structural bonding including check of kiss-bonding and heterogeneity in the adhesive joint. For such investigation, we propose to use the infrared thermography technique as this convenient technology allows the acquisition of thermal surface field without contact. Then representative data of the physical mechanism involved inside the material, such as internal decohesion, may be deduced [10]. By this methodology, we intend to study the adhesion between the primary structure and the composite patch as well as its structural efficiency under mechanical solicitations (damage tracking [11]).

The weak thickness of the adhesive joint and the similar thermal characteristics between composite matrix and glue make difficult the determination of heterogeneities. To address such issue, it is essential to define first the current limits of infrared thermography. In this way, we propose to study here the influence of a heat load on the thermal response acquired by infrared thermography. Several materials are studied, either isotropic (metallic) or anisotropic (composites), in order to identify the heat flow sent by a light source. After the presentation of materials, we describe the experimental bench settled for the present study. Then the heat flow identification procedure is detailed, combined with the numerical modelling used. Results are presented in a last part.

2 Materials

Regarding the repair process, the final goal is to investigate carbon-epoxy composite laminates bonded in form of two step lap elementary coupons (figure 1). Before addressing such complex issue, we intend to characterize macroscopically homogeneous materials ("reference materials") for which physical and thermal characteristics are well-known :

- two metallic coupons with different thicknesses: stainless steel with a thickness of $1.9\,\mathrm{mm}$ and Inconel with a thickness of $0.9\,\mathrm{mm}$,
- two carbon fiber reinforced plastics (CFRP) made of 18 plies of epoxy resin M10 and T300 fibers (prepreg manufactured by Hexcel) cured in an autoclave; two different lay up have been considered, namely $[0]_{18}$ and $[0/90/0]_6$) (both have a thickness of $4.7\,\mathrm{mm}$).

Reference coupons of $125\,\mathrm{mm}$ length and $85\,\mathrm{mm}$ width have been machined by laser (metallic materials) and by water jet (composites).

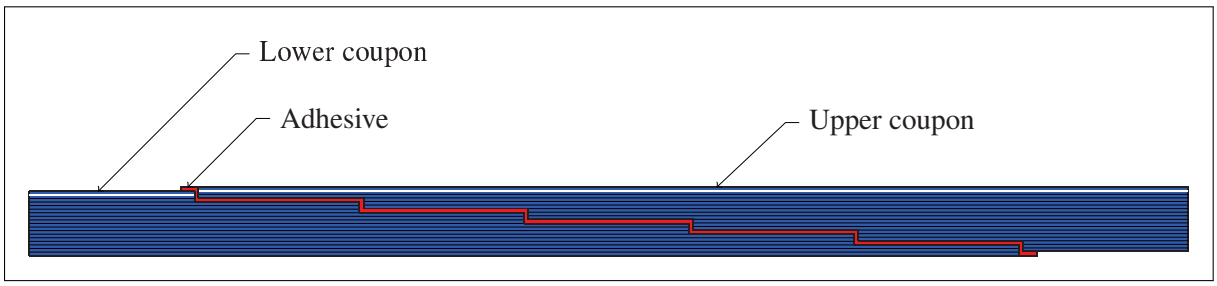

Figure 1: Assembly of two elementaries coupons

3 Experimental setup

3.1 Requirements

The aim is to acquire by means of infrared thermography the temperature fields on the surface of thermally loaded samples. Thermography can be used with two experimental configurations, in transmission (figure 2a) or in reflexion (figure 2b). The transmission set up consists of having the heat source in the opposite side of the camera. For the reflection configuration, the heat source and the camera stand in the same side. Thermal mapping measured by the camera corresponds to the flow reflected by the material

surface. This configuration has been considered in the present study as it may provide a higher resolution and depth quantification. Moreover, it is more relevant in an industrial context when only one side of the specimen is available [12].

For several years, many studies related to the Non Destructive Testing (NDT) by infrared thermography have been done in the LGP laboratory on composites materials [10, 13]. Following equipment is classically used: a HAMEG signal generator that controls a PULSAR signal amplifier, an halogen lamp (120 V 1000 W), a CEDIP Infrared camera JADE retrofitted in FLIR Titanium (20 mK resolution, MW 50 mm lens) and ALTAIR software (for film capture and results visualization/analysis).

Regarding the reflection configuration, four parameters can influence the experimental results: the distance and angle between lamp and coupon (D_l and α on figure 2b), the signal form (rectangular, square and sinus) and amplitude. In order to determine their respective influence, it is essential to characterize the amplitude of the signal sent by the light source. The latter is controlled by the HAMEG signal generator and the real thermal heat flow emitted by the lamp is not yet known. Besides, first investigations based on the existing NDT device highlight several problems for the present application case (figure 3). Especially, we note that the halogen lamp provides a divergent heat flow which cannot focus on the coupon center and that the position of this heat flow cannot be precisely controlled (figure 3a). Also, the sample holder made in aluminium creates a heat sink (figure 3b) and reflects the thermal heat flow on the reference coupon (figure 3b). Finally, the geometric position of the lamp, the camera and the sample are not perfectly defined, so it is difficult to completely control the heat flow impact on the sample.

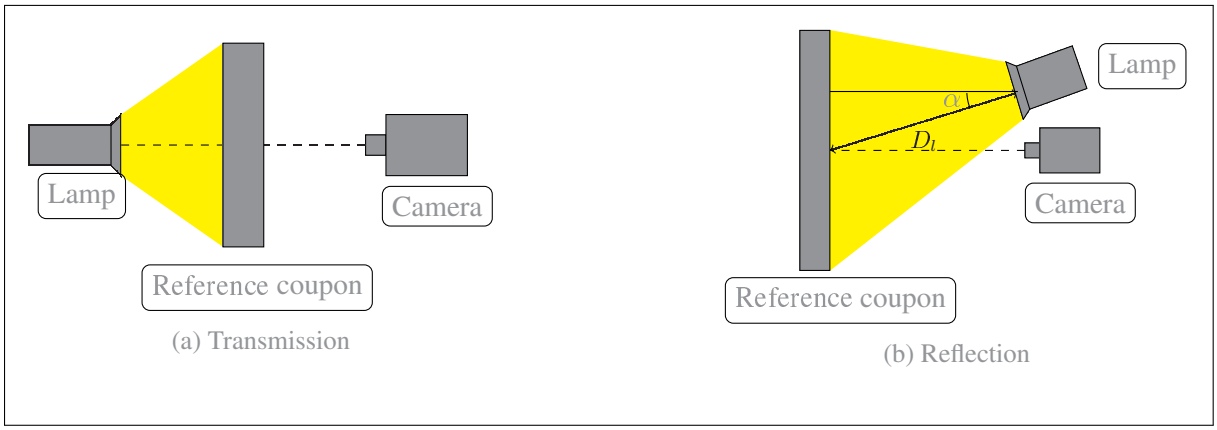

Figure 2: Infrared thermography setups

3.2 New experimental bench

According to previous difficulties, it was thus necessary to create a specific experimental bench to handle tests with best controlled conditions. The first aim was to generate a localized and parallel light flow for the heat load of the sample. To transform the divergent heat flow of the halogen into a parallel flow, a set of optical lenses is used (figure 4). Behind the lamp outlet, a shutter is placed to reduce the heat flow diameter and a divergent lens is used to reduce the global bench dimensions. A convergent lens then concentrates the heat flow on its optical point. After this point, the heat flow diverges again and another convergent lens finally allows to transform the divergent heat flow into parallel flow. Distances between different elements and focal lengths of lens provide a thermal loaded area in agreement with further investigations.

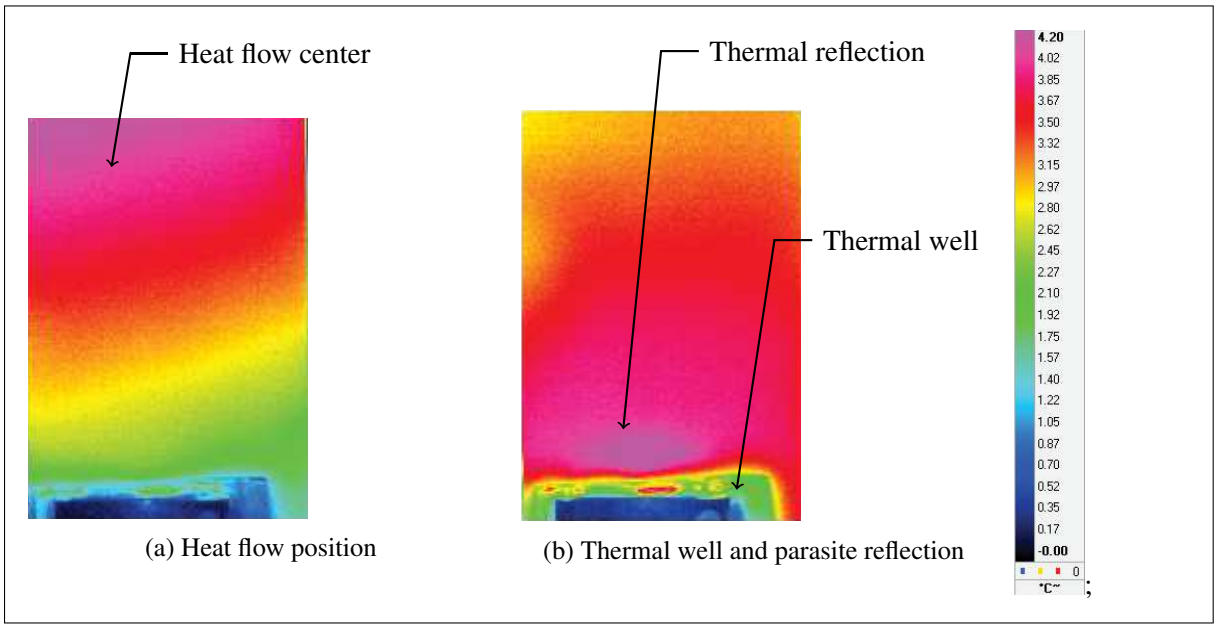

(a) Heat flow position

(b) Thermal well and parasite reflection

Figure 3: Difficulties related to existing NDT device (inconel sample)

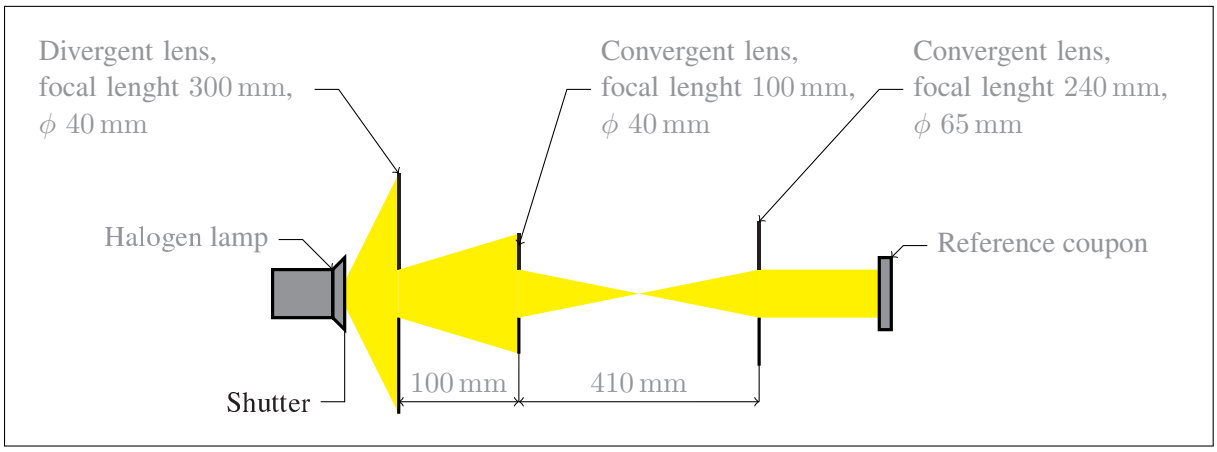

Figure 4: Schematic drawing of the heat flow

To control geometric positions of sample, lamp, and camera, a test bench was designed (figure 5). It allows to check the distance (from the shutter) between the halogen lamp and sample, the angle between the heat flow and the sample and to keep the camera axis normal to the stimulated face of the sample.

Then, it was necessary to control the thermal boundary conditions on the samples and, specially, avoid thermal well and parasite reflection induced by the aluminium handler of samples (figure 3b). Accordingly, we have chosen to put an insulating material (cross-linked PVC Airex C70) on the back face of these samples (figure 6c), with larger lenght than specimen and which is itself handled at the bottom part by the aluminium handler. A Sicomin SR1126 epoxy glue with hardener SD8205 was used to paste the two parts. To ensure maximal glue thickness of 0.1 mm, a calibrated film of Teflon is inserted between the reference coupon and its support (figure 6b).

Finally, the transcription in temperature of the radiation captured by the infrared camera requires the

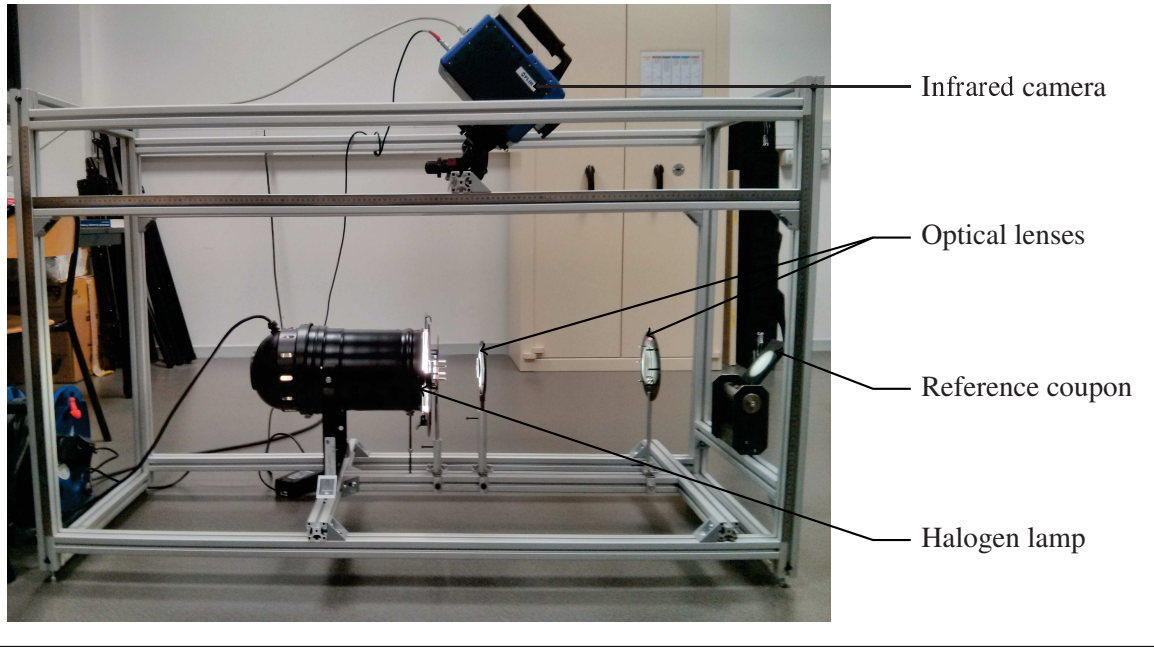

Figure 5: Test bench

(a) Polished reference coupons, inconel (left) and stainless steel (right)

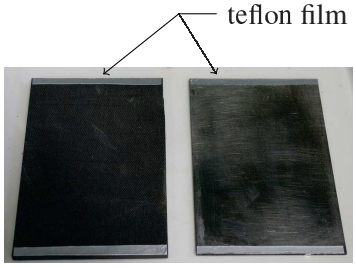

(b) Application of a calibrate film, CFRP $[0]_{18}$ (left), Inconel (right)

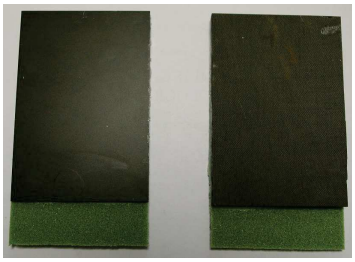

(c) Glued and painted reference coupon on their support, Inconel (left), CFRP $[0]_{18}$ (right)

Figure 6: Preparation of samples

knowledge of the material emissivity. This parameter corresponds to the ratio between the tested material and a reference body said black body. A precise estimation of that parameter remains quite difficult. In this way, metallic coupons were thinly polished (figure 6a) and all samples were painted in mat black (figure 6c), so as to consider an uniform and constant value of emissivity corresponding to carbon (0.98).

3.3 Load conditions and experimental features

Regarding the load, samples are thermally stimulated by a rectangular signal for $10\,\mathrm{s}$ (figure 7a). The heat flow is centered and elliptical in shape (figure 7b). Since light rays are parallel after the last convergent lens, the width of the heat flow area remains constant with angle α of $25°$; on the contrary, the height of the ellipse grows with α (table 1).

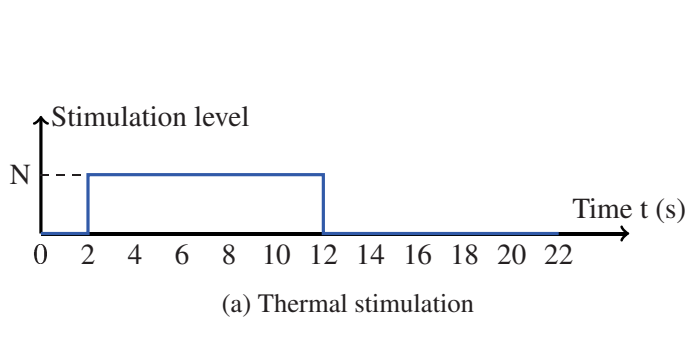

(a) Thermal stimulation

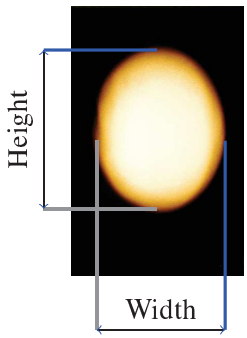

(b) Heat flow area for an angle between lamp and reference coupon of $45°$

Figure 7

α (°)	Width (mm)	Height (mm)
0	58	58
25	58	64
30	58	68
40	58	77

Table 1: Heat flow area variation in function of angle between lamp and reference coupon

Acquisition by infrared thermography is done up to the end of the relaxation phase (22 s) with an acquisition frequency fixed to $f = 50\,\mathrm{Hz}$. After acquisition, a data processing is set up to provide the relative temperature variation fields $\Delta T = T - T_0$ over the sample, with T the temperature field at time t and T_0 the temperature field in the initial state $t = 0$. The relative analysis allows to avoid disturbing and environmental effects and to enhance the thermal response of studied sample.

Figure 8 shows relative temperature fields obtained for tested materials for a given configuration ($D_l = 800\,\mathrm{mm}$, $\alpha = 25°$). It should be noted that the temperature variation obtained for stainless steel is very low. Indeed, this material exhibits a similar diffusivity $D = \dfrac{\lambda}{\rho C_p}$ as Inconel but its thickness is twice and heat rapidly decrease. Related thermal measurements are thus very disturbed by the camera noise itself. Thermal increase observed for others materials is more important, even if hot points are less than $2\,°\mathrm{C}$. Given a measurement area in the hotest part of their surface, one can calculate the spatial mean temperature variation for such area. Figure 9 demonstrates the good repeatability for such quantity of different tests on a same material.

4 Heat flow identification

4.1 FEMU technique

The determination of the heat flow provided by the halogen lamp is done on isotropic materials by Finite Element Model Updating (FEMU) between experimental thermal fields and numerical modelling. According to previous results, Inconel is used for such identification as thermal heterogeneities are more

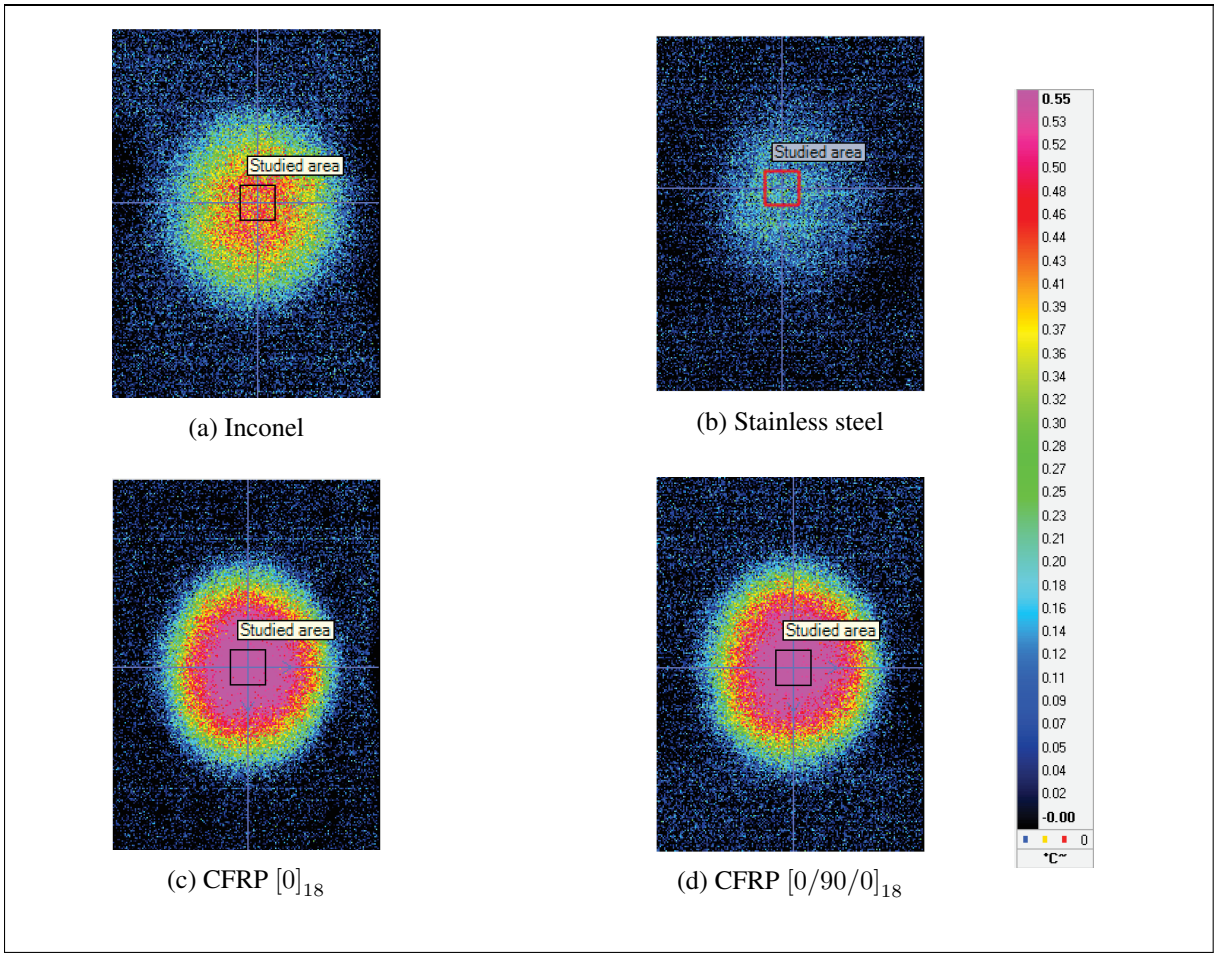

(a) Inconel

(b) Stainless steel

(c) CFRP $[0]_{18}$

(d) CFRP $[0/90/0]_{18}$

Figure 8: Relative thermal fields at a time of $t = 6\,\mathrm{s}$ ($D_l = 800\,\mathrm{mm}$, $\alpha = 25°$)

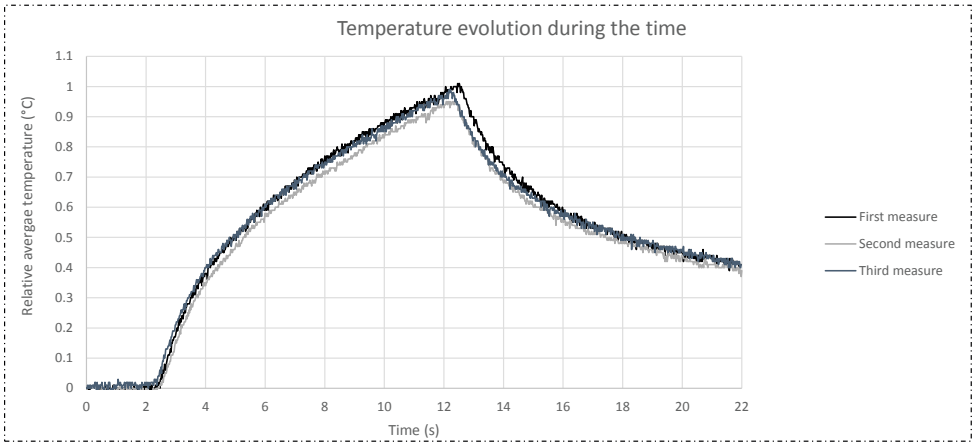

Figure 9: Spatial relative average temperature on the measurement area for three tests on $[0]_{18}$ CFRP ($D_l = 800\,\mathrm{mm}$, $\alpha = 25°$)

notable. In a second step, we intend to test the value obtained to the case of anisotropic composites materials.

FEMU technique is based on the least square method to compare experimental thermal surface response to the numerical response (figure 10). For experimental tests and numerical results, we use the spatial average relative temperature on the measurement area at two instants (time $t_{r1} = 8\,\mathrm{s}$ and time $t_{r2} = 12\,\mathrm{s}$). In view of discrete and noisy experimental data, a time average of measured temperature around these instants is taken into account for the experimental response (including $t = t_r - 2\Delta t$, $t = t_r - \Delta t$, $t = t_r$, $t = t_r + \Delta t$, $t = t_r + 2\Delta t$ with $\Delta t = \dfrac{1}{f} = 0.02\,\mathrm{s}$). Once the difference between experimental and numerical responses is sufficiently low (distance D defined at equation 1), the thermal surface heat flow is checked.

$$D = \sum_{i}^{2} \sqrt{\left(m_{num,(tri)} - m_{exp(tri)}\right)^2} \tag{1}$$

with m the spatial average temperature on the studied area.

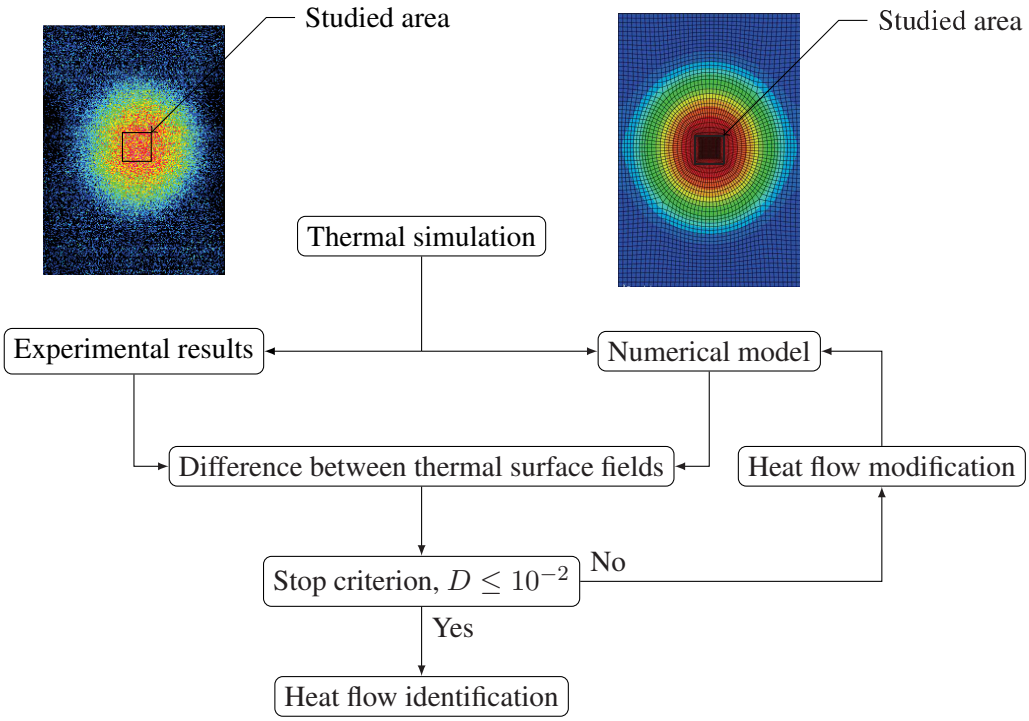

Figure 10: Inverse characterization method

4.2 Numerical model

Assumptions taken into account to create the numerical modelling are the following ones:

1. Inconel, glue and Airex C70 are considered as isotropic and CFRP plies are considered as transversely isotropic (all properties of materials are provided in table 2). The transversal isotropic behaviour of CFRP plies is deduced from thermal conductivities of fibers and epoxy resin [14]. Direction 1 corresponds to fiber direction and directions 2 and 3 to transverse one;

2. The ambient temperature is considered as steady and uniform in the whole room and is measured before every test;

3. For measured temperatures, the radiation is neglected;

4. The thermal convection coefficient for a vertical plate with a length under $30\,\mathrm{cm}$ can be calculated with the following equation [15]:

$$h_c = 1.42 \left(\frac{\Delta T}{H} \right)^{0.25} \tag{2}$$

where ΔT is the temperature difference between the sample surface and the ambient temperature and H is the plate length. Natural convection is implemented in the model for waiting and relaxation phase but not in the heat flow application area for the stimulation phase;

5. The contact between the reference coupon and its support is considered as perfect (no air between reference coupon and its support);

6. A surface heat flow is applied on an elliptic area of $58\,\mathrm{mm}$ wide and variable height (in function of the angle between the heat flow and the sample, table 1).

	Stainless steel	Inconel	C70	Glue	Composite ply
Density ρ, $[\mathrm{kg\,m^{-3}}]$	$8000^{(a)}$	$8650^{(a)}$	$75^{(b)}$	$1155^{(a)}$	$1450^{(b)}$
Specific heat Cp, $[\mathrm{J\,kg^{-1}\,K^{-1}}]$	$500^{(a)}$	$490^{(a)}$	$1130^{(a)}$	$1660^{(a)}$	$1000^{(a)}$
Conductivity λ, $[\mathrm{W\,m^{-1}\,K^{-1}}]$	$16^{(a)}$	$17^{(a)}$	$0.03^{(b)}$	$0.2^{(a)}$	$\lambda_1 = 5.8^{(c)}$ $\lambda_2 = \lambda_3 = 0.85^{(c)}$
Thermal diffusivity D, $[\mathrm{m^2\,s^{-1}}](10^{-6})$	4	4.01	0.35	0.1	$D_1 = 4$ $D_2 = D_3 = 0.58$

Table 2: Physical and thermal properties of materials provided by Granta CES data software (a), manufacturers (b) or homogenization technique (c)

Inconel and CFRP $[0]_{18}$ reference coupons are obtained by cutting the whole assembly with a partition tool. Next, materials are attributed to the different partitions. CFRP $[0]_{18}$, which is constituted of plies with the same direction, exhibits physical and thermal properties of the composite ply. On the contrary, all plies of the CFRP $[0/90/0]_6$ are modelled including their respective fiber direction. To mesh the assembly with an optimum efficiency, diffusive heat transfer element types which care of thermal diffusion and convection (DCC3D8) are used. Moreover, a convergence survey is automatically settled for all reference coupons (see table 3).

	Inconel	CFRP $[0]_{18}$	CFRP $[0/90/0]_6$
Number of mesh elements	21 047	32 868	87 114

Table 3: Numbers of mesh elements for different reference materials

4.3 Resuts

With a power of $575\,\mathrm{W}$ provided by the halogen lamp for the considered configuration ($D_l = 800\,\mathrm{mm}$, $\alpha = 25°$), the heat flow transmitted by the test bench (lamp and lens set) is identified to $0.87\,\mathrm{W\,m^{-2}}$ on Inconel (figure 11a). Application of such identified heat flow to composite materials leads to a good correlation between numerical simulation and experimental results.

One could note also that the temperature increase and decrease for Inconel sample are linear (figures 11a) contrary CFRP (figures 11b and 11c). Such difference can be explained by the material symmetry and shows that the anisotropic thermal behavior of composites clearly leads to a much more complex non linear response to a thermal load.

Good behaviour on ascending phase temperature can be observed between experimental and numerical, which allows to validate the device and procedure developed in this work. The maximum deviation is observed on CFRP $[0]_{18}$ at the end of acquisition (at $t = 22\,\mathrm{s}$) and is equal to $1.69\,\%$, whereas a maximal deviation of $1.23\,\%$ on the $[0/90/0]_6$ CFRP is obtained at just after the end (at $t = 13\,\mathrm{s}$) of the thermal solicitation.

5 Conclusion and perspectives

In this work, an experimental bench allowing thermal tests under controlled conditions has been designed. An identification procedure based on FEMU technique has been settled and provides a reliable quantification of thermal heat flow. Subsequent studies will now be based on these results with the aim of defining the influence of geometrical parameters, amplitude and form of the source signal on the temperature fields. From this, tests will be carried out in order to define the current observation limits of infrared thermography for repaired bonded structures. In that case such inspection, it may be required to include trackers into the glue joint (such as boron nitrite [4, 16]) so as to enhance the specific response of the glue joint and thus to improve the inspection of bonded interfaces.

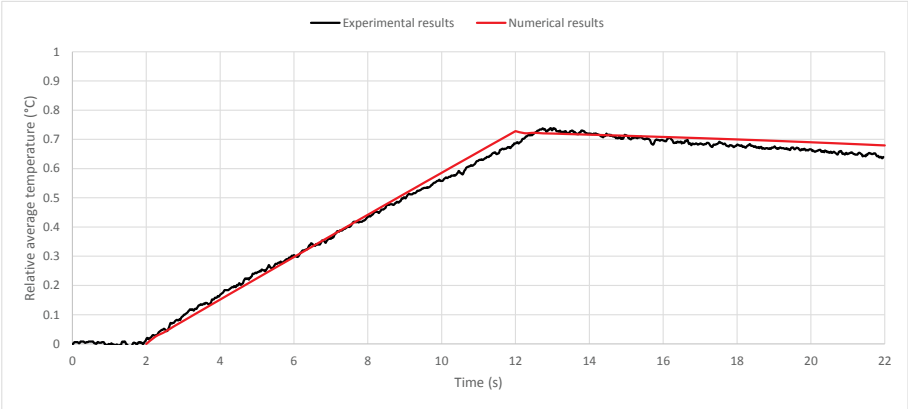

(a) Inconel

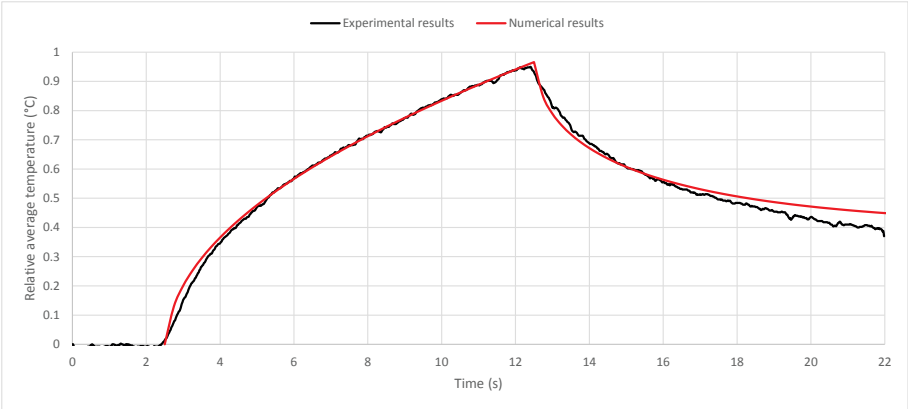

(b) CFRP $[0]_{18}$

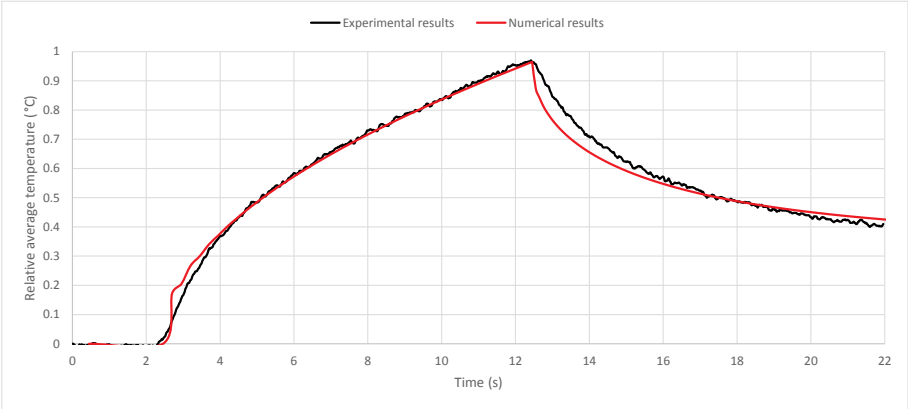

(c) CFRP $[0/90/0]_6$

Figure 11: Spatial relative average temperature on the measurement area for reference coupons (numerical simulation uses heat flow identified on Inconel material)

References

[1] K. Wood. In-situ composite repair build basics. http://www.compositesworld.com/articles/in-situ-composite-repair-builds-on-basics, 2008.

[2] G. Goulios and Z. Marioli-Riga. Composite patch repairs for commercial aircraft: Compres. *Air & amp; Space Europe*, 3(3):143–147, 2001.

[3] J. Rouchon. Bonded composite patches in front of civil airworthiness requirements. In *Composite Patch Repair Seminar*. DGA Techniques Aéroanutique, 2007.

[4] JJ Wang, RT Zheng, JW Gao, and G Chen. Heat conduction mechanisms in nanofluids and suspensions. *Nano Today*, 7(2):124–136, 2012.

[5] L. Ilcewicz, L. Cheng, J. Hafenricher, and Ch. Seaton. Guidelines for the development of a critical composite maintenance and repair issues awareness course. Technical Report DOT/FAA/AR-08/54, FAA: Federal Aviation Administration, 2009.

[6] X. Liu and G. Wang. Progressive failure analysis of bonded composite repairs. *Composite Structures*, 81(3):331 – 340, 2007.

[7] R. D. Adams and D. Robert. *Adhesive bonding: science, technology and applications*. Elsevier, 2005.

[8] S. Guibert. La thermographie infrarouge à détection synchrone appliquée aux matériaux composites. Master's thesis, Université Laval, Québec, 2007.

[9] C. Soutis and F.Z. Hu. Design and performance of bonded patch repairs of composite structures. *Proceedings of the Institution of Mechanical Engineers, Part G: Journal of Aerospace Engineering*, 211(4):263–271, 1997.

[10] E. Peronnet, M.L. Pastor, R. Huiller, O. Dalverny, S. Mistou, and H. Welemane. Non destructive investigation of defects in composite structures by three infrared thermographic techniques. In *ICEM15*. Porto, 2012.

[11] M.L. Pastor, X. Balandraud, M. Grédiac, and J.L. Robert. Applying infrared thermography to study the heating of 2024-t3 aluminium specimens under fatigue loading. *Infrared Physics & amp; Technology*, 51(6):505–515, 2008.

[12] C. L. Castanedo. *Quantitative subsurface defect evaluation by pulsed phase thermography: depth retrieval with the phase*. PhD thesis, Université Laval, 2005.

[13] C. Garnier, M.L. Pastor, F. Eyma, and B. Lorrain. The detection of aeronautical defects in situ on composite structures using non destructive testing. *Composite structures*, 93(5):1328–1336, 2011.

[14] B. Valès. Caractérisation thermo mécanique de l'endommagement des composites stratifiés par thermograhie infrarouge. Master's thesis, Université de Bourgogne, Institut Supérieur de l'Automobile et des Transports, 2013.

[15] B. Eyglunent. Manuel de thermique (revue et pratique). *Hermes, Paris*, pages 277–290, 1997.

[16] W. L. Song, P. Wang, L. Cao, A. Anderson, M. J. Meziani J, A. J Farr, and Y. P. Sun. Polymer/boron nitride nanocomposite materials for superior thermal transport performance. *Angewandte Chemie International Edition*, 51(26):6498–6501, 2012.